Development of mutated β-catenin gene signature to identify *CTNNB1* mutations from whole and spatial transcriptomic data in patients with HCC
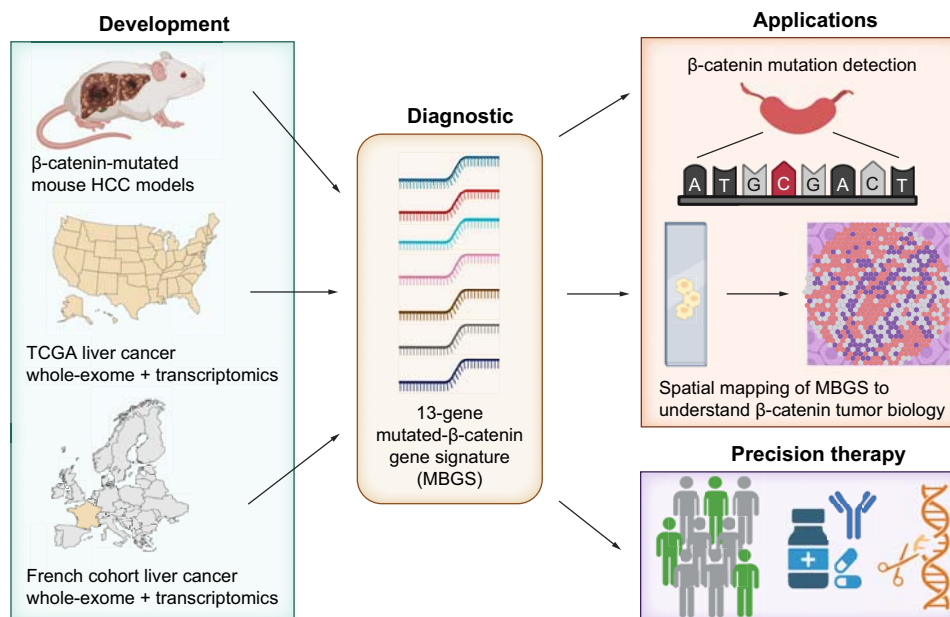
Authors

Brandon M. Lehrich, Junyan Tao, Silvia Liu, …, Jessica Zucman-Rossi, Yulei Wang, Satdarshan P. Monga

Correspondence

smonga@pitt.edu (S.P. Monga).

Graphical abstract

Highlights:

- We developed a 13-gene mutated-β-catenin gene signature (MBGS) through transcriptomic analysis of β-catenin-mutated and wild-type HCC mouse models.

- The MBGS predicted CTNNB1-mutated patients with ROC AUC of 0.90 to 0.94 in multiple HCC patient cohorts.

- Spatial transcriptome mapping of MBGS revealed β-catenin-mutated HCCs were immune excluded.

- MBGS has potential as a companion diagnostic for precision medicine for patients with HCC.

Impact and implications:

As precision medicine for liver cancer treatment becomes a reality, diagnostic tools are needed to help classify patients into groups for the best treatment choices. We have developed a molecular signature that could serve as a companion diagnostic and uses bulk or spatial transcriptomic data to identify a unique subclass of liver tumors. This subgroup of liver cancer patients derive limited benefit from the current standard of care and are expected to benefit from specialized directed therapies that are on the horizon.

Development of mutated β-catenin gene signature to identify *CTNNB1* mutations from whole and spatial transcriptomic data in patients with HCC

Brandon M. Lehrich[1,2,3], Junyan Tao[1,2], Silvia Liu[1,2], Theo Z. Hirsch[4,5], Tyler M. Yasaka[1,2,3], Catherine Cao[1], Evan R. Delgado[1,2], Xiangnan Guan[6], Shan Lu[6], Long Pan[4,5], Yuqing Liu[1], Sucha Singh[1], Minakshi Poddar[1], Aaron Bell[1,2], Aatur D. Singhi[7], Jessica Zucman-Rossi[4,5], Yulei Wang[6], Satdarshan P. Monga[1,2,8,*]

Check for updates

Background & Aims: Patients with β-catenin (encoded by *CTNNB1*)-mutated hepatocellular carcinoma (HCC) demonstrate heterogenous responses to first-line immune checkpoint inhibitors (ICIs). Precision-medicine based treatments for this subclass are currently in clinical development. Here, we report derivation of the Mutated β-catenin Gene Signature (MBGS) to predict *CTNNB1*-mutational status in patients with HCC for future application in personalized medicine treatment regimens.

Methods: Co-expression of mutant-Nrf2 and hMet ± mutant-β-catenin in murine livers in mice led to HCC development. The MBGS was derived using bulk RNA-seq and intersectional transcriptomic analysis of β-catenin-mutated and non-mutated HCC models. Integrated RNA/whole-exome-sequencing and spatial transcriptomic data from multiple cohorts of patients with HCC was assessed to address the ability of MBGS to detect *CTNNB1* mutation, the tumor immune microenvironment, and/or predict therapeutic responses.

Results: Bulk RNA-seq comparing HCC specimens in mutant β-catenin-Nrf2, β-catenin-Met and β-catenin-Nrf2-Met to Nrf2-Met HCC model yielded 95 common upregulated genes. In The Cancer Genome Atlas (TCGA)-LIHC dataset, differential gene expression analysis with false discovery rate (FDR) = 0.05 and $\log_2$(fold change) >1.5 on the 95 common genes comparing *CTNNB1*-mutated *vs.* wild-type patients narrowed the gene panel to a 13-gene MBGS. MBGS predicted *CTNNB1*-mutations in TCGA (n = 374) and French (n = 398) patient cohorts with AUCs of 0.90 and 0.94, respectively. Additionally, a higher MBGS expression score was associated with lack of significant improvement in overall survival or progression-free survival in the atezolizumab-bevacizumab arm *vs.* the sorafenib arm in the IMbrave150 cohort. MBGS performed comparable or superior to other *CTNNB1*-mutant classifiers. MBGS overlapped with Hoshida S3, Boyault G5/G6, and Chiang CTNNB1 subclass tumors in TCGA and in HCC spatial transcriptomic datasets visually depicting these tumors to be situated in an immune excluded tumor microenvironment.

Conclusions: MBGS will aid in patient stratification to guide precision medicine therapeutics for *CTNNB1*-mutated HCC subclass as a companion diagnostic, as anti-β-catenin therapies become available.

Introduction

Liver cancer, of which hepatocellular carcinoma (HCC) is the most common, is the third leading cause of cancer-related death worldwide.[1] The global burden is projected to increase as the etiology shifts from viral to nonviral causes, including alcoholic liver disease and metabolic dysfunction associated steatotic liver disease.[2] HCC develops in the background of these chronic liver diseases as liver injury and inflammation drive fibrosis, cirrhosis, and eventually cancer. In the advanced disease setting, overall survival (OS) is 12–18 months with current systemic therapy.[3] Existing immunotherapeutic combinations with immune checkpoint inhibitors (ICIs) have drastically improved the treatment armamentarium for HCC, however, objective response rates remain critically low between 30–35%.[4,5] Early *post-hoc* analysis has indicated that both tumor genetics and tumor microenvironment features likely influence ICI response.[6]

One such pathway with known heterogenous ICI response rates observed in preclinical models and in patients with HCC is the Wnt/β-catenin pathway.[7,8] In HCC, approximately 26–37% of patients, depending on the geographic region, harbor mutations in *CTNNB1,* the gene encoding β-catenin.[9,10] These mutations are stabilizing, gain-of-function (GOF) mutations mostly in exon 3 of the *CTNNB1* gene. In adults, β-catenin

ELSEVIER

EASL™
The Home of Hepatology

under normal physiological conditions (in the absence of Wnt ligand) is phosphorylated, ubiquitinated, and degraded by the proteasomal degradation machinery. However, mutations render β-catenin unable to be phosphorylated or ubiquitinated, which leads to its stabilization and nuclear translocation to act as a transcription co-factor with TCF/LEF family members to turn on target gene expression. We and others have demonstrated a role for β-catenin in tumor cell proliferation and growth,[11,12] tumor metabolism[13,14] and tumor-immune interactions.[8] Identifying patients with β-catenin activation thus may have direct prognostic and therapeutic implications in HCC as treatment becomes more personalized.[6]

As tissue and/or liquid biopsy continues to augment the diagnostic landscape for HCC, utilizing molecularly targeted therapies in combination with ICI are likely to improve response rates.[15] Thus, to translate this therapeutic combination into clinical practice, animal models which recapitulate the complex molecular biology driven by specific genetic drivers, rather than random combinations of oncogenes, in an immunocompetent mouse background, are needed to improve our understanding of the cellular and molecular basis of this disease. Our lab utilizes sleeping beauty transposon/transposase and hydrodynamic tail vein injection (SB-HDTVI) to transfect mouse hepatocytes *in vivo* with various combinations of oncogenes to mimic human HCC subsets. Using this 'inside-out' model, we have determined that the introduction of β-catenin alone does not initiate tumorigenesis, but rather requires cooperation with other secondary drivers to induce tumors in mice.[12] Specifically, we have previously shown that mutated-β-catenin cooperates with hMET and Nuclear-factor-like 2 (NRF2) to induce HCC, with each model representing 9-12% of human HCC subsets.[12,14] Thus, further development of these models may provide novel opportunities to understand tumor biology, biomarker discovery, and test therapeutics.

In the current study, we identified approximately 14% of HCC cases that demonstrate concomitant activation of NRF2 and MET signaling. In addition, a subset of these patients had GOF mutations in *CTNNB1*. Based on these clinical observations, we co-expressed mutant-*CTNNB1* ± mutant-*NRF2* and *hMET* using SB-HDTVI, which induced HCC development in mice. Transcriptomic profiling of multiple tumors demonstrated similarity to the respective human HCC subsets. With the availability of a multitude of HCC mouse models with transcriptomic data, we were able to derive a common gene signature representing β-catenin activity referred henceforth as the **M**utant **β**-catenin-specific **G**ene **S**ignature (MBGS) which was verified in its ability to successfully identify CTNNB1-mutated HCC in multiple patient cohorts. Additionally, we demonstrate comparable or superior performance of MBGS to other molecular subclass gene signatures and Wnt/β-catenin gene signatures in both whole and spatial transcriptomic datasets. Tumor nodules which demonstrate high MBGS expression are immune excluded, yet may be situated within an inflamed stroma. This illustrates that β-catenin likely drives tumor immune exclusion within nodules, but other tumor extrinsic features direct immune activity within the stroma. Overall, our study has derived a transcriptomic signature with expected value in patient molecular stratification for personalized medicine in HCC as a companion diagnostic when anti-β-catenin therapies become available.

Results

Significant subsets of patients with HCC have overlapping NRF2 and MET gene signatures and represent a distinct molecular subgroup

We have previously identified cooperativity between β-catenin and NRF2 activation and between β-catenin and MET activation, using patient HCC samples and in mouse models with each subset representing around 9-12% of all HCCs.[12,14] Here, we investigated whether NRF2 and MET co-activation cooperate in the pathogenesis of HCC, and whether this could be modeled *in vivo* to study liver tumor biology of such a distinct subset. First, to determine whether a subgroup of patient tumors have any overlap in NRF2 and MET activation, we extracted datasets from the Cancer Genome Atlas (TCGA) of liver hepatocellular carcinoma (LIHC) patients.[10] TCGA data contained a total of 374 HCC cases including 50 cases for which adjacent normal tissues are also available. To define a population of patients that were NRF2-active (henceforth referred to as NRF2-high), we applied hierarchical clustering to the entire cohort using a previously published 28-gene NRF2 activation gene signature,[16] which grouped the cases into 4 distinct clusters as we have previously described (Fig. S1a).[14] The cluster identified 100 HCC cases with high expression of the 28-gene NRF2 activation gene signature, suggesting ∼27% of all HCC cases to be NRF2-high, which encompassed the majority of patients with HCC with GOF-mutations in *NFE2L2* or loss of function (LOF)-mutations in *KEAP1*, but also captured cases with NRF2 activation independent of these mutations. Additionally, to define a population of patients which were MET-active (henceforth referred to as MET-high), we applied hierarchical clustering to the entire TCGA-LIHC cohort using the previously published KAPOSI_LIVER_CANCER_MET_UP 18-gene signature[17] from mSigDB (Fig. S1b), as we have previously described using a smaller TCGA cohort.[12,18] Interestingly, we observed a dichotomous sub-clustering of the 18-gene MET activation signature, where we defined a cluster representing patients with high expression of the top nine genes on the heatmap, and a cluster representing patients with expression of the bottom nine genes on the heatmap. Thus, we classified the MET-high patients as those in both clusters combined (pink and green in Fig. S1b), representing 175 patients with HCC, or ∼47% of all HCC cases. From this analysis, we also observed that many patients included in these clusters had GOF-mutations in *NFE2L2* or LOF-mutations in *KEAP1*, suggesting potential cooperativity between NRF2 and MET (Fig. S1b). Indeed, we identified 54 patients with HCC or 14.4% of all HCC cases, which showed an overlap of NRF2-high and MET-high gene signatures in TCGA (Fig. 1a).

Differential gene expression analysis, comparing the 54 NRF2/MET-high patients to the 50 normal tissue cases in TCGA-LIHC cohort, yielded 5,238 differentially expressed genes (DEGs) by false discovery rate (FDR) = 0.001 and absolute log fold change (logFC) >3 (Table S1). Ingenuity pathway analysis (IPA) was performed on 5,238 DEGs and identified 254 significantly enriched pathways (Table S2), with the top 10 altered pathways depicted to notably be cell cycle checkpoints, Kinetochore metaphase signalling, and others (Fig. 1b, Table S2). Thus, concomitant NRF2 and MET activation is apparent in a significant subset of patients with HCC.
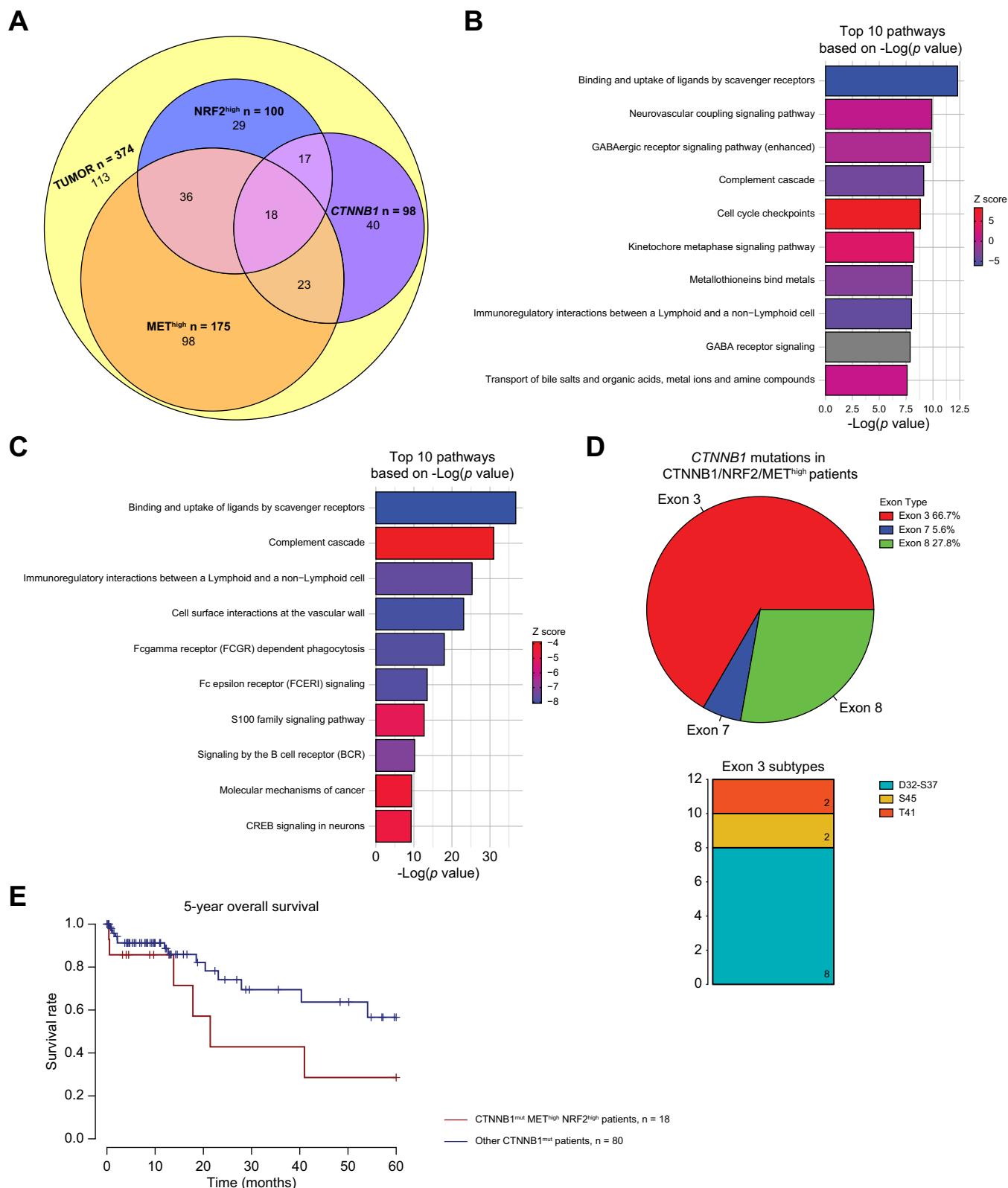
Fig. 1. Influence of Nrf2 and Met pathway activation on gene expression in HCC with and without CTNNB1-mutations. (A) Venn diagram of 374 The Cancer Genome Atlas-Liver Hepatocellular Carcinoma (TCGA-LIHC) patients categorized as Nrf2-high, Met-high, or CTNNB1-mutated, and their patient overlap. Eighteen (4.8% all HCC) patients had overlap of *CTNNB1*-mutation, Nrf2-high, Met-high. (B) Top 10 pathways based on *p* value from Ingenuity pathway analysis (IPA) of differentially expressed genes comparing patients categorized as Nrf2-/Met-high (n = 54) *vs.* normal (n = 50). Specifically, 5,238 differentially expressed genes were applied to IPA analysis with cutoff of false discovery rate (FDR) = 0.001 and absolute logFC >3. (C) Top 10 pathways based on *p* value from IPA of differentially expressed genes comparing patients categorized as CTNNB1-mutated/Nrf2-/Met-high (n = 18) *vs.* normal (n = 50). Specifically, 5,114 differentially expressed genes

Distinct subset of HCCs with overlapping NRF2/MET-high gene signature harbor CTNNB1 mutations with a unique transcriptome and more aggressive phenotype

Given the cooperativity of β-catenin and NRF2 and between β-catenin and MET, we hypothesized that a subset of NRF2/MET-high patients may also harbor *CTNNB1* mutations. In TCGA-LIHC cohort, 98 patients had mutations in *CTNNB1*. We identified 35 (9.4%) cases with CTNNB1-mutation/NRF2-high overlap and 41 (10.9%) had CTNNB1-mutation/MET-high overlap.[12,14] In addition, among the 54 TCGA-LIHC NRF2-high/MET-high patients, 18 patients, or 4.8% of all HCC cases, had mutations in *CTNNB1* (Fig. 1a). Interestingly, of these 18 patients, 12 patients (67%) had mutations in exon 3, five (28%) had mutations in exon 8, and one patient had a mutation in exon 7 (Fig. 1d, Fig. S1c). In addition, of the 12 patients with exon 3 mutations, eight (67%) belonged to D32-S37 subgroup, two (17%) patients were S45 subgroup, and two (17%) patients were the T41 subgroup (Fig. 1d), with the D32-S37 subgroup having the highest β-catenin activity, T41 moderate activity, and S45 the weakest activity (although with gene duplication) based on previous genotype-phenotype analysis.[19] Thus, 18.4% (n = 18/98) of all *CTNNB1*-mutated HCC cases had an NRF2-high/MET-high gene signature, and majority of these cases had *CTNNB1* point mutations with high β-catenin activity.

Differential gene expression (DGE) analysis, comparing the 18 *CTNNB1*-mut/*NRF2*/*MET*-high patients to the 50 normal tissue cases in TCGA-LIHC cohort, yielded 5,114 DEGs by FDR = 0.001 and absolute log FC >3 (Table S3). IPA was performed on the 5,114 DEGs and 261 significantly enriched pathways were identified (Table S4), with the top 10 pathways summarized in Fig. 1c. Additionally, given that we identified many patients showing high β-catenin activity (the majority in the D32-S37 subgroup), we queried whether the tumors in these patients exhibited a more aggressive phenotype. Indeed, the 18 *CTNNB1*-mutant/NRF2/MET-high patients trended towards a worse OS as compared with all other *CTNNB1*-mutated patients (n = 80) (p = 0.104) (Fig. 1e). However, when comparing *CTNNB1*-mutant/NRF2/MET-high (n = 18) to CTNNB1-wild-type/NRF2/MET-high patients (n = 36), OS showed no differences (Fig. S2a), suggesting that within NRF2/MET-high patients, CTNNB1-mutation is not influencing survival. It appears NRF2 is trending to be a driver of poorer survival in *CTNNB1*-mutated cases, although no statistical significance was evident (Figs. S2b and c). Studies in larger cohorts are needed to extent these findings.

Concomitant expression of mutant-GOF β-catenin with mutant-GOF NFE2L2 and hMET in a subset of murine hepatocytes in vivo induces tumors with early morbidity and mortality

We have previously shown that single oncogene induction of either GOF-mutant *CTNNB1*, GOF-mutant *NFE2L2*, or *hMET* does not induce HCC in mice.[12,14] Thus, to model *in vivo* our observations in clinical cohorts of patients with HCC, we forced expression of S45Y-CTNNB1 ± G31A-NFE2L2 ± hMET in 6-week-old FVB male mice through hydrodynamic tail vein injection (HDTVI) with sleeping beauty transposon/transposase, as previously described (Fig. 2a).[12,14] Mice injected with S45Y-CTNNB1 + G31A-NFE2L2 + hMET (β-N-M) displayed signs of early morbidity and mortality by ∼5 weeks post-HDTVI compared with other β-catenin driven models and mice injected with G31A-NFE2L2 + hMET (N-M) (Fig. 2b). This aggressive phenotype mirrored survival analysis from the clinical cohort (Fig. 1e). At the ∼5-week timepoint, we observed livers with notable gross HCC and significantly increased liver weight (LW)/body weight (BW) ratio of ∼15% (p <0.001) compared with 4-5% LW/BW in wild-type FVB (Fig. 2c, Fig. 2e). Histologically, these nodules were large, well-circumscribed, and well-differentiated HCC foci with trabecular pattern, minimal nuclear atypia, and moderate fatty changes (Fig. S3a). Microscopically, we observed >80% HCC were simultaneously positive for Myc-tag (representing mutant *CTNNB1*), Nqo1 (NRF2 target), and V5-tag (representing hMET) (Fig. S3a).

The N-M mice showed progressive morbidity by 14 weeks post-HDTVi, with significantly longer survival compared with the β-N-M, β-N, and β-M models (Fig. 2b). At the 14-week timepoint, the livers had gross macroscopic tumor nodules with LW/BW ratio of 9–12%, which was significantly greater (p <0.001) than 4-5% in the wild-type FVB mice (Fig. 2d, e). Histologically, these nodules were moderately-sized, well-circumscribed, and well-differentiated HCC with trabecular patterns, minimal nuclear atypia, and minimal fatty change (Fig. S3b). The nodules were dually positive for Nqo1 and V5-tag (Fig. S3b). This suggested that the tumors in the N-M model stemmed from concomitant activation of NRF2 and hMET. Additionally, immunohistochemistry (IHC) for Ki67, which stains proliferating cells, demonstrated that models with β-catenin activation tended to be more proliferative (Fig. S4).

Lastly, to confirm the activation of β-catenin and its downstream targets in the β-N-M model, we performed IHC for β-catenin, demonstrating its nuclear translocation as compared with its membranous localization in the wild-type FVB mice (Fig. 2f). We also observed β-N-M tumor nodules were glutamine synthetase (GS) and cyclin D1-positive (Fig. 2f). The tumor nodules in the N-M model stained negative for nuclear β-catenin and lacked intra-tumoral GS staining, with minimal cyclin D1-positive nuclei, suggesting lack of β-catenin activity in this model (Fig. 2f). Overall, the β-N-M model demonstrates an aggressive β-catenin-driven model compared with other β-catenin-driven models, and the N-M model lacked any β-catenin activity.

Murine tumors with mutant-GOF β-catenin were transcriptionally distinct from tumors without β-catenin activation

Next, we performed transcriptional analysis on tumors from mutant-β-catenin models (β-N-M model, n = 3; β-M model, n =

were subjected to IPA analysis with cutoff of FDR = 0.001 and absolute logFC >3. For both (A) and (B) ranking of pathways based on -log(p value) and activation/inhibition of pathway determined by z-score. Percentages and frequencies are shown. (D) (Left) Pie chart depicting the distribution of exon mutations and (Right) stacked bar plot depicting the frequency of different exon 3 mutations in CTNNB1-mutated/Nrf2-/Met-high patients. (E) Kaplan-Meier curve showing trending decreased overall survival (OS) in CTNNB1-mutated/Nrf2-/Met-high (n = 18) compared with other CTNNB1 mutated cases (n = 80). Log-rank test p = 0.104. Levels of significance: p <0.05, **p <0.001, ***p <0.0001.
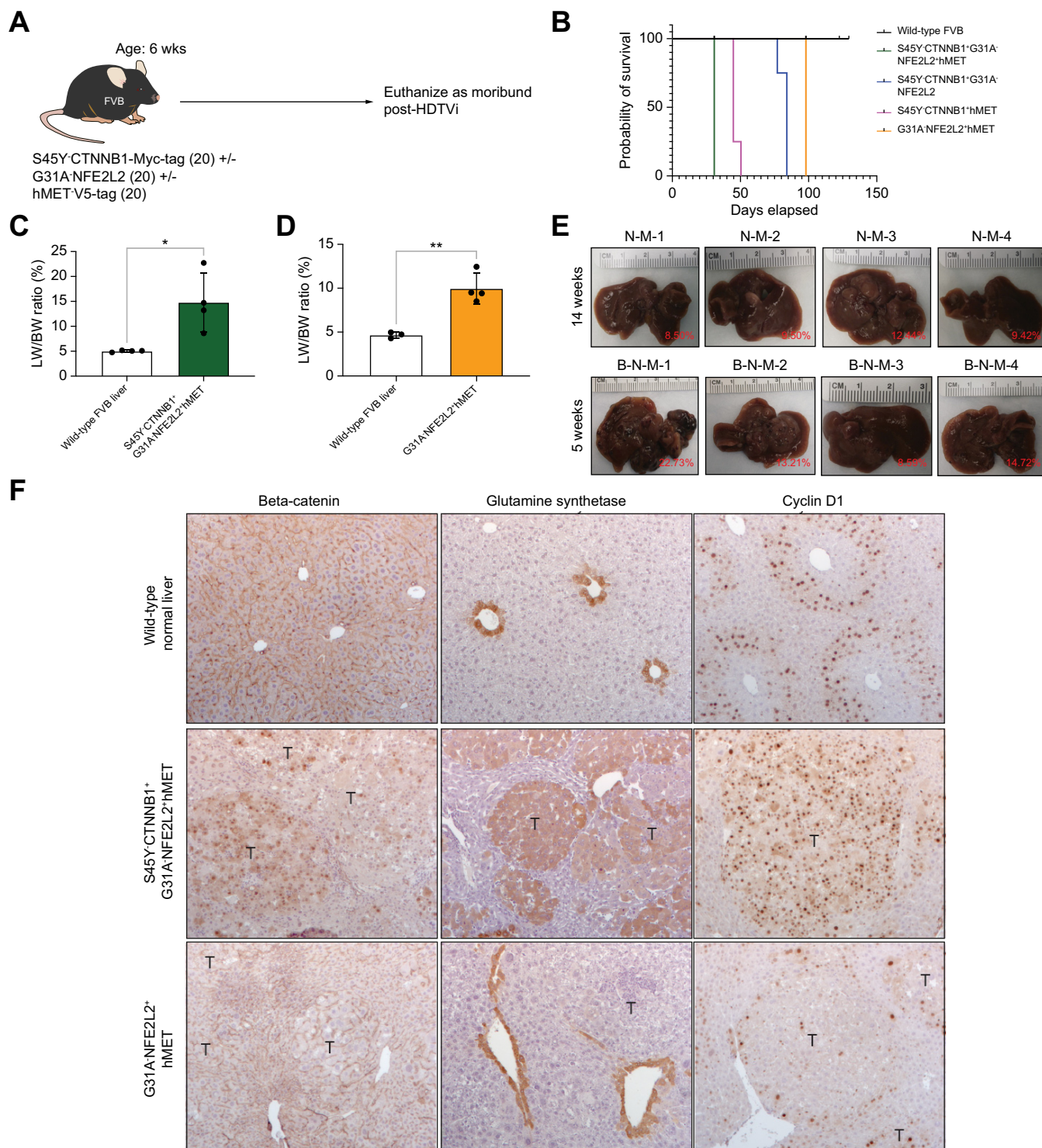
Fig. 2. **Establishing murine liver cancer models of mutated-CTNNB1 with or without mutated-NFE2L2 and hMET.** (A) Schematic showing the timeline of sleeping beauty transposon/transposase with hydrodynamic tail vein injection (SB-HDTVi) of S45Y-CTNNB1 with or without G31A-NFE2L2 and hMET in 6-week-old FVB mice. (B) Kaplan-Meier curve showing decreased survival of S45Y-CTNNB1-G31A-NFE2L2-hMET compared with G31A-NFE2L2-hMET mice. Log-rank test p <0.0001 for global comparisons. (C) Bar graph shows significant increase in liver weight (LW)/body weight (BW) ratio in S45Y-CTNNB1-G31A-NFE2L2-hMET mice compared with wild-type FVB liver at same timepoint of euthanasia (Student's t-test *p = 0.0159). (D) Bar graph showing significant increase in LW/BW ratio in G31A-NFE2L2-hMET mice compared with wild-type FVB liver at the same timepoint of euthanasia (Student's t-test; **p = 0.0036). For both (C) and (D) bars represent standard deviation and individual data points are plotted with top of the bar representing the mean. (E) Macroscopic images of the whole livers from S45Y-CTNNB1-G31A-NFE2L2-hMET and G31A-NFE2L2-hMET at 14-weeks (upper panel) and ∼5-week (lower panel) post injection. Gross images suggest presence of advanced liver tumors in each group. LW/BW ratio for each picture shown as percentage in red in the image. (F). Immunohistochemistry shows tumor foci to be positive for β-catenin targets glutamine synthetase (GS) and Cyclin D1 in S45Y-CTNNB1-G31A-NFE2L2-hMET (middle panel) compared with G31A-NFE2L2-hMET (lower panel). Levels of significance: *p <0.05, **p <0.001, ***p <0.0001.
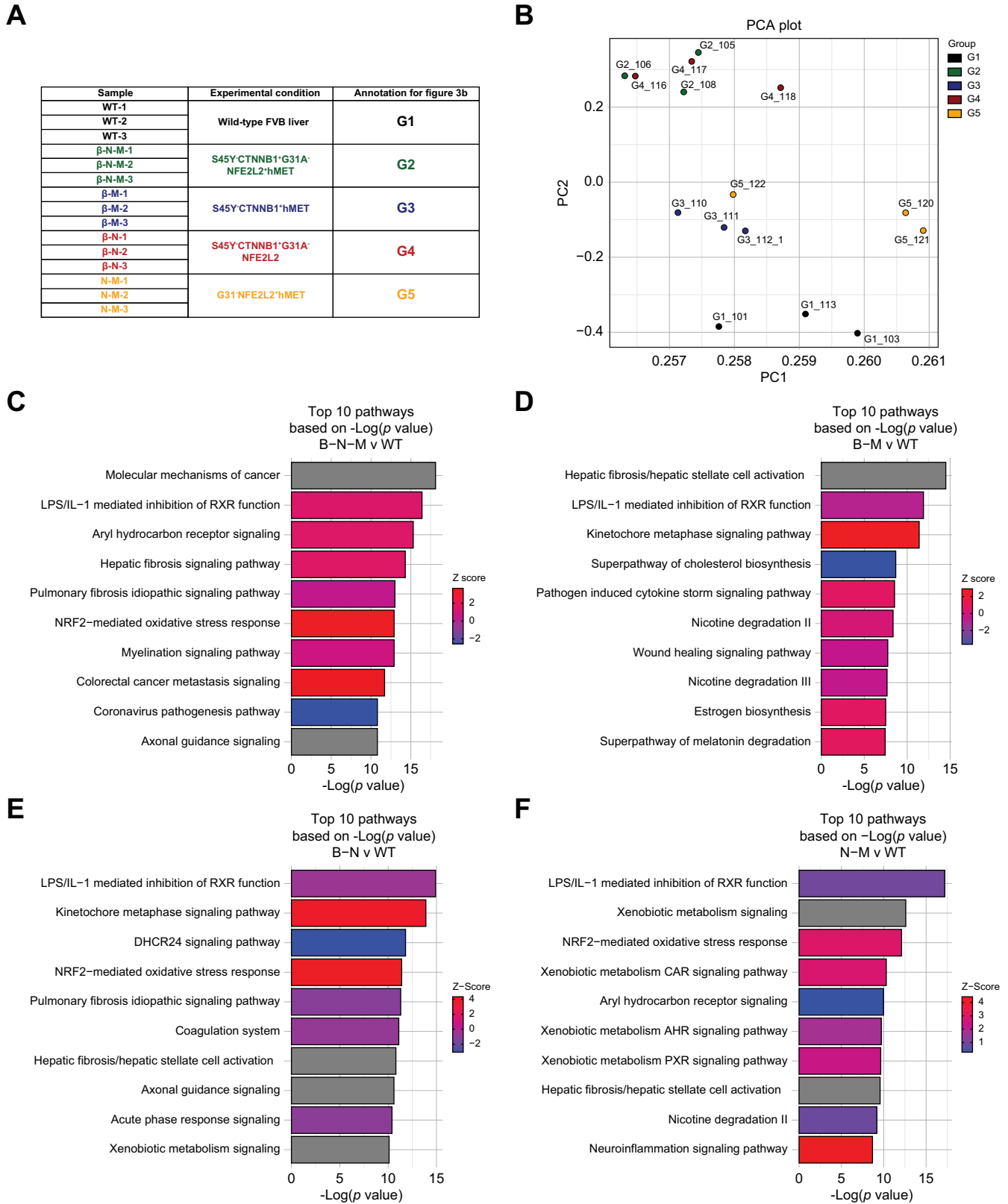
Fig. 3. Transcriptomic analysis of multiple β-catenin-mutated and non-mutated models reveals differences in gene expression. (A) Description of the samples used for transcriptomic analysis. Each mouse tumor model had three replicates sequenced. (B) Principal component analysis demonstrates clustering of wild-type distinct from the tumor models, with models of high Met activity clustering similarly and models of high Nrf2 activity clustering similarly. (C) Top 10 pathways based on *p* value from ingenuity pathway analysis (IPA) of differentially expressed genes comparing S45Y-CTNNB1-G31A-NFE2L2-hMET to wild-type. Specifically, 4,577 differentially expressed genes were applied to IPA analysis with cutoff of false discovery rate (FDR) = 0.05 and absolute log fold change >1.5. (D) Top 10

3; β-N model, n = 3) and a non-β-catenin model (N-M model, n = 3) to compare with the normal mouse liver (wild-type [WT] FVB livers, n = 3) to identify tumor-enriched pathways in each model (Fig. 3a). Principal component analysis on the 15 samples showed WT clustered distinctly from all the tumor models (β-N-M, β-M, β-N, and N-M). Liver tumors from mice clustered similarly between β-N-M and β-N, while β-M and N-M clustered similarly (Fig. 3b). To identify putative gene signatures in each tumor-bearing model, DGE was determined by comparing the WT liver to each tumor model (β-N-M, β-M, β-N, and N-M). Briefly, we identified 2,627 upregulated genes and 1,950 downregulated genes comparing WT *vs.* β-N-M selected by FDR = 5% and absolute log FC >1.5 (Fig. S5a). Pathway analysis on the DEGs identified activation of Aryl hydrocarbon receptor signalling, Kinetochore metaphase signaling, and NRF2-mediated oxidative stress response, among others (Fig. 3c; Table S5). DGE analysis identified 1,016 upregulated genes and 527 downregulated genes comparing WT *vs.* β-M (Fig. S5b) and 2,405 upregulated genes and 1,950 downregulated genes comparing WT *vs.* β-N (Fig. S5c) with similar *post-hoc* statistical corrections. Additionally, pathway analysis comparing WT *vs.* β-M (Fig. 3d; Table S6) and WT *vs.* β-N (Fig. 3e; Table S7) identified relevant previously described pathways.[12,14] Interestingly, we also identified 1167 upregulated genes and 697 downregulated genes comparing WT *vs.* N-M models (Fig. S5d). Here, pathway analysis on the DEGs identified activation of relevant pathways, including NRF2-mediated oxidative stress response, Xenobiotic metabolism, Hepatic fibrosis signalling, and Glutathione redox reactions, among others (Fig. 3f; Table S8).

Murine tumors with NRF2/MET co-expression ± CTNNB1 mutation showed high transcriptional similarity to respective human HCC subsets with similar molecular perturbations

We have previously shown that the T41A-CTNNB1-G31A-NFE2L2 model and the S45Y-CTNNB1-hMET model have 77% and 70% transcriptional similarity, respectively, to human patients with HCC with the same molecular alterations.[12,14] To determine transcriptional similarity of both the β-N-M and N-M models to respective human HCCs with similar perturbations, DGE and IPA were determined and compared (see Supplemental Methods). Overlapping the mouse DGE to human orthologs yielded 970 and 2,377 common genes for NRF2/MET-high and *CTNNB1*-mutant/NRF2/MET-high patient groups, respectively, with the DGE for each depicted on the heatmap (Figs. S6a and b). Next, we compared the transcriptional overlap quantitatively between the mouse models and human HCC and found high correlation of *CTNNB1*-mutant/NRF2/MET-high (0.807 by Pearson's correlation analysis; Fig. S7a) and NRF2/MET-high (0.758 by Pearson's correlation; Fig. S7b). Additionally, there were 261 and 430 significantly

enriched pathways in human and mouse *CTNNB1*-mutant/NRF2/MET-high, respectively, of which 124 were common between mice and humans, with the top enriched pathways shown in Fig. S7c. Lastly, there were 254 and 252 significantly enriched pathways in human and mouse NRF2/MET-high respectively, of which 69 were common between the mice and patients, with the top enriched pathways shown in Fig. S7d. Overall, our analysis demonstrates that the mouse models well represent the human HCC subsets with similar molecular alterations, and thus provide a platform to develop biomarkers and test therapies.

Comparison of mutant-GOF β-catenin models to N-M model identifies a mutated β-catenin gene signature
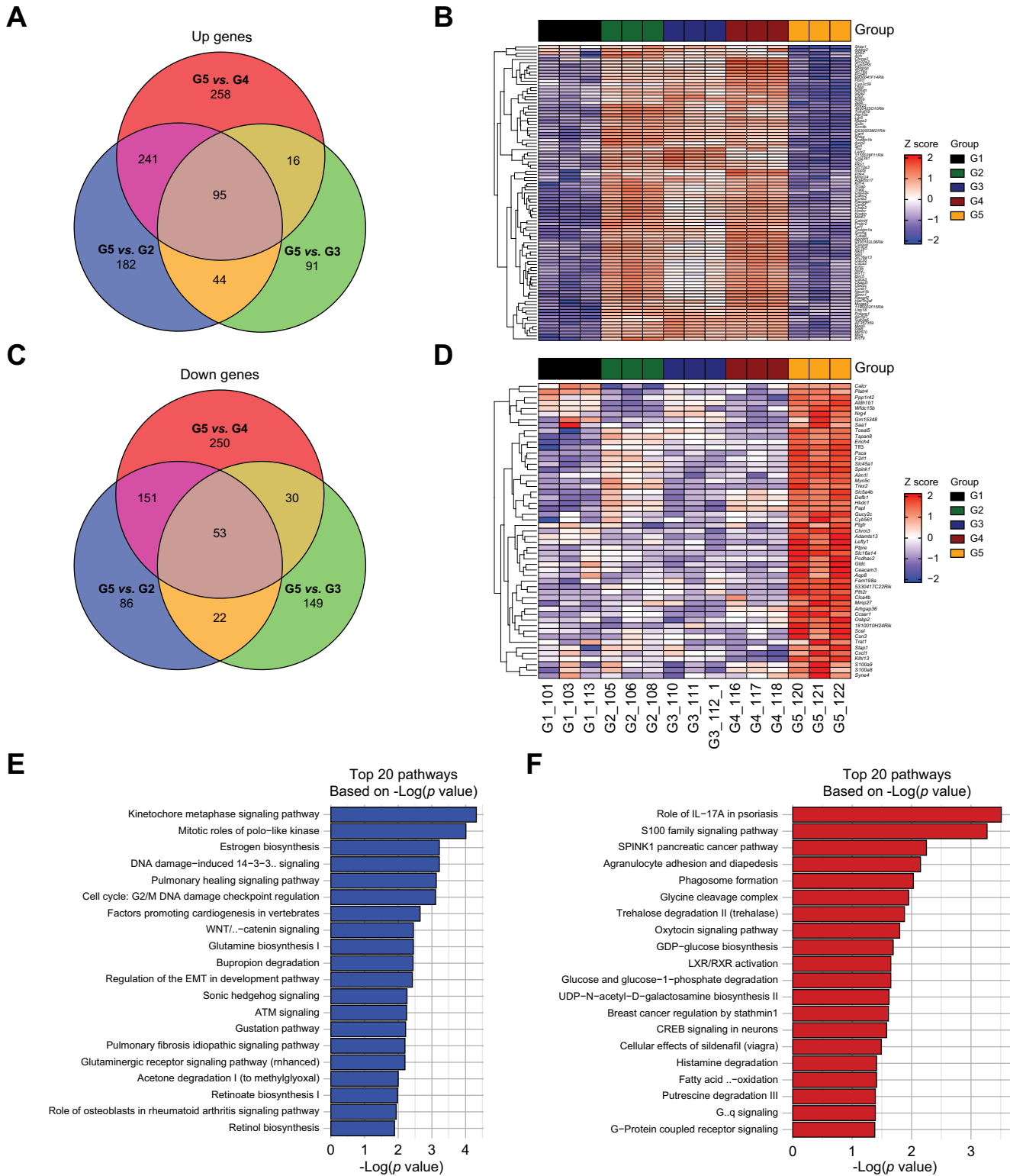
Since we had transcriptomic data available from multiple clinically relevant models with and without β-catenin mutation using combinations of the same set of oncogenes, we attempted to derive a gene signature specific to β-catenin activity in HCC. First, we performed DGE analysis with the following model comparisons: N-M *vs.* β-N-M (Fig. S8a), N-M *vs.* β-M (Fig. S8b), and N-M *vs.* β-N (Fig. S8c), to allow comparison of each β-catenin mutated model to the β-catenin wild-type model, and then overlapped the common DEGs, defined as FDR = 0.05 and absolute logFC >3 to identify the common upregulated (95 genes) (Fig. 4a) and downregulated genes (53 genes) (Fig. 4c), followed by IPA for each of the model comparisons (Figs. S9a–c). The 95 upregulated and 53 downregulated genes were visualized on heatmaps with the upregulated genes demonstrating high expression (Fig. 4b), and the downregulated genes demonstrating low expression (Fig. 4d), in all β-catenin driven models. IPA on the 95 upregulated genes identified pathways enriched for Glutamine biosynthesis, Wnt/β-catenin signalling, Glutaminergic receptor signalling, and Retinol/retinoate biosynthesis (Fig. 4e). IPA on the 53 downregulated genes identified pathways enriched for S100 family signalling pathway, Agranulocyte adhesion and diapedesis, and Phagasome formation (Fig. 4f). Thus, β-catenin active tumors are enriched in glutamine signaling,[13] as we have previously shown, and retinol/retinoate signaling, as others have shown to be potential mechanisms of ICI response in solid tumors.[20]

MBGS identified patients with CTNNB1 mutations

Of the 95 enriched mouse genes, 85 mapped 1:1 to human orthologs in TCGA-LIHC cohort. In TCGA-LIHC dataset, the z-scores based on normalized and scaled expression values of the 85 human genes were visualized on heatmap with three clusters: adjacent normal (n = 50), *CTNNB1*-wild-type (n = 276), and *CTNNB1*-mutated (n = 98) (Fig. S10). We next performed DGE analysis on these 85 human genes comparing CTNNB1-wild-type to CTNNB1-mutated cases with cut-off of FDR = 0.05 and absolute logFC >1.5, and identified 13 differentially

Fig. 4. Transcriptomic analysis comparing β-catenin-mutated to non-mutated models identifies β-catenin specific gene expression signatures. (A) Common 95 upregulated genes comparing the three β-catenin-mutated models to the G31A-NFE2L2-hMET model based on differential gene expression with cutoff of false discovery rate (FDR) = 0.05 and absolute log$_2$ fold change >3. (B) Heatmap of 95 upregulated genes shows high expression in each of the three β-catenin-mutated models compared with the G31A-NFE2L2-hMET model. Normalized and scaled gene expression based on z-score is shown. (C) Common 53 downregulated genes comparing the three β-catenin-mutated models to the G31A-NFE2L2-hMET model based on differential gene expression with cutoff of FDR = 0.05 and absolute log$_2$ fold change >3. (D) Heatmap of 53 downregulated genes shows low expression in each of the three β-catenin-mutated models compared with the G31A-NFE2L2-hMET model. Normalized and scaled gene expression based on z-score is shown. (E) Top 20 pathways based on *p* value from ingenuity pathway analysis (IPA) of the 95 common upregulated genes from (A). (F) Top 20 pathways based on *p* value from IPA of the 53 common downregulated genes from (C). For (E, F) ranking of pathways based on -log(*p* value). G1: wild-type liver; G2: S45Y-CTNNB1-G31A-NFE2L2-hMET; G3: S45Y-CTNNB1-hMET; G4: S45Y-CTNNB1-G31A-NFE2L2; G5: G31A-NFE2L2-hMET.

expressed genes, which were upregulated in CTNNB1-mutated HCC cases: *AXIN2, GLUL, LGR5, NKD1, NOTUM, RHBG, SBSPON, SLC13A3, SLC1A2, SP5, TCF7, TEDDM1,* and *TNFRSF19*, which comprised our 13-gene MBGS (Fig. 5a). These were also visualized on heatmap comparing expression between normal and CTNNB1-mutated and wild-type cases (Fig. 5b). We next compared expression of individual genes in normal, CTNNB1-wild-type, and CTNNB1-mutated tissues. We observed that SLC1A2 had higher expression in normal tissue; and, TEDDM1 and SBSPON were only expressed in subset of CTNNB1-mutated HCC cases (Fig. 5c). Thus, we also formalized a reduced 10-gene MBGS to include only *AXIN2, GLUL, LGR5, NKD1, NOTUM, RHBG, SLC13A3, SP5, TCF7,* and *TNFRSF19*.

Next, we wanted to determine whether the 13- and 10-gene MBGS had predictive ability to classify TCGA-LIHC patients with CTNNB1 mutations. We assessed the composite average expression of the 13-gene (Fig. 6a) and 10-gene (Fig. 6b) MBGS panels in normal, CTNNB1-wild-type, and CTNNB1-mutated tissues. In TCGA-LIHC, the 13-gene and 10-gene MBGS had predictive ability to classify CTNNB1-mutated cases with AUC of 0.91 and 0.90, respectively, and the sensitivity and specificity of the 13-gene MBGS was 0.857 and 0.877, respectively (Fig. 6c). We also assessed the predictive ability of CTNNB1-mutation status with composite average expression of other molecular subclasses of gene signatures known to overlap with patients harboring CTNNB1 mutations, along with previously published Wnt gene signatures using TCGA-LIHC dataset. Boyault G5/G6,[21] Chiang CTNNB1 subclass,[22] Hoshida S3,[23] and Lachenmayer Wnt-CTNNB1[24] gene signatures predicted *CTNNB1* mutational status with AUCs of 0.9013 (sensitivity: 0.837; specificity: 0.891), 0.8983 (sensitivity: 0.867; specificity: 0.837), 0.5898 (sensitivity: 0.969; specificity: 0.203), and 0.8892 (sensitivity: 0.776; specificity: 0.931), respectively (Figs. S11a–h). Additionally, BIOCARTA_WNT_PATHWAY, KEGG_WNT_SIGNALING_PATHWAY, and REACTOME_SIGNALING_BY_WNT_IN_CANCER predicted *CTNNB1* mutational status with AUC of 0.6299 (sensitivity: 0.489; specificity: 0.743), 0.5877 (sensitivity: 0.918; specificity: 0.301), and 0.6008 (sensitivity: 0.439; specificity: 0.743), respectively (Figs. S12a–f).

We additionally tested the expression of this signature in another HCC cohort of 398 cases from France.[25] Expression of the 13-gene and 10-gene MBGS was assessed in normal (n = 31), *CTNNB1*-wild-type (n = 280), and *CTNNB1*-mutated (n = 118) cases and showed significant enrichment of the signature in *CTNNB1*-mutated cases (Fig. 6d, e). In the French cohort, the 13-gene and 10-gene MBGS had predictive ability to classify CTNNB1-mutated cases with AUC of 0.95 and 0.94, respectively (Fig. 6f). In addition, the average expression of MBGS was assessed in patient groups stratified by Boyault G1-G6 subgroup status,[21] and demonstrated enrichment in G5/G6 subgroups, as this subgroup is enriched for *CTNNB1*-mutated and active tumors (Fig. 6g, h). We also identified that MBGS is specific to predicting *CTNNB1*-mutated patients compared with other molecular subclass predictions (Boyault, Hoshida, Chiang), as can be seen in the heatmap overlapping all subclasses, *CTNNB1*-mutated patients, and MBGS expression by all 13-genes (Fig. S13). Thus, we successfully developed a 13-gene panel to identify CTNNB1-mutated HCCs across multiple patient cohorts with superior or comparable performance to previously reported molecular subclasses or Wnt-CTNNB1 gene signatures.

MBGS classified tumors with β-catenin mutations in pan-cancer atlas

We were also interested in determining whether MBGS would be able to classify non-HCC liver tumors with Wnt/β-catenin pathway activity, including hepatocellular adenoma and hepatoblastoma. We first observed that MBGS was mostly enriched in patients with HCC with exon 3 mutations (Figs. S14a and b). Additionally, we observed enrichment of MBGS in both hepatocellular adenomas (n = 6) and hepatoblastomas with *CTNNB1* alterations, accounting for patients with either mutations in *CTNNB1* (n = 92) or biallelic APC mutations (n = 4) (Figs. S14a and b). Next, we utilized the pan-cancer atlas which integrates transcriptomic-exome data from ICGC/TCGA cases with 2,565 patients across 2,683 samples of multiple tumor types (Fig. S15a), of which 178 harbored mutations in *CTNNB1*. Our 10-gene signature was able to classify CTNNB1-mutated tumors with an AUC of 0.703 (Fig. S15b). Overall, MBGS had greater liver specificity and additional targets that are tumor- or tissue-type specific may be needed to further improve its performance.

MBGS predicts fewer immunotherapy related treatment effects in patients with HCC

Given the discrepant studies associating Wnt/β-catenin pathway activation and ICI response in HCC,[6,26] we were interested in how MBGS expression would prognosticate treatment effects in immunotherapy treated cohorts. We first analyzed a previously reported smaller HCC dataset including 17 patients with eight responders and nine non-responders who received ICIs.[27] Uniform Manifold Approximation and Projection (UMAP) demonstrated gene expression separation of responders and non-responders (Fig. S16a). DGE analysis showed that many of the MBGS genes were downregulated in responders *vs*. non-responders (Fig. S16b). These genes were enriched in non-responders (Fig. S16c). Comparison of MBGS to previously published 175-gene CHIANG_LIVER_CANCER_SUBCLASS_CTNNB1_UP[22] to predict ICI response resulted in similar AUCs of 0.78 and 0.79, respectively (Figs. S16d–g). We also compared MBGS to other previously reported ICI response gene signatures, including the T cell-inflamed gene expression profile,[28] the IFNg response signature,[29] and the tertiary lymphoid structure (TLS) signature,[30] with these demonstrating AUCs of 0.68, 0.71, and 0.72, respectively (Figs. S17a–c).

We also assessed whether MBGS expression levels mirrored the results observed in *CTNNB1*-mutated patients in the IMbrave150 cohort,[6] in which fewer atezolizumab/bevacizumab (atezo/bev)-specific treatment effects were observed in *CTNNB1*-mutated compared with *CTNNB1*-WT patients. In the IMbrave150 cohort, both the 13- and 10-gene MBGS correlated with each other and were enriched in *CTNNB1*-mutated cases (Fig. 7a–c). Interestingly, in patients receiving atezo/bev, expression of MBGS did not prognosticate OS or progression-free survival (PFS) (Fig. 7d, e). In addition, in patients with higher MBGS expression, improved OS or PFS was observed in the sorafenib arm, illustrating the rationale for observed fewer treatment effects in MBGS high *vs.* low cohorts

Fig. 5. Transcriptomic analysis of mouse-specific β-catenin activated genes in TCGA-LIHC identifies mutated-β-catenin gene signature (MBGS). (A) Volcano plot of differentially expressed genes comparing *CTNNB1*-mutated (n = 98) *vs. CTNNB1*-wild-type (n = 276) The Cancer Genome Atlas-Liver Hepatocellular Carcinoma (TCGA-LIHC) cases using the 85 human orthologs of the 95 mouse genes based on differential gene expression with cutoff of false discovery rate (FDR) = 0.05 and absolute log fold change >1.5. (B) Heatmap of the 13 differentially expressed in TCGA-LIHC showing enrichment of the genes in *CTNNB1*-mutated cases. Normalized

comparing atezo/bev *vs.* soraenib arms. Specifically, patients with low expression of MBGS showed clinical improvement with atezo/bev compared with sorafenib in terms of OS (p = 0.0329) and PFS (p = 0.0293) (Figs. S18a and b), which was likely attributed to fewer treatment effects of sorafenib in MBGS low compared with high patients. We further stratified clinical response using mRECIST criteria for complete/partial response (CR/PR), stable disease (SD), and progressive disease (PD) in each treatment arm and by MBGS expression. Higher MBGS expression was associated with CR/PR or SD in sorafenib arm compared with lack of association in atezo/bev arm (Fig. 7f), illustrating that patients with CTNNB1 activity derive significant clinical benefit from sorafenib but are not associated with primary resistance to combination ICI. Thus, using MBGS expression levels as a surrogate readout are able to mirror the results observed in the IMbave150 cohort when profiling *CTNNB1* mutational status.

Spatial mapping of molecular subclass signatures identifies tumor intrinsic and extrinsic features with MBGS depicting immune excluded tumors

Lastly, given that *CTNNB1*-mutated patients have previously been reported to have an immune excluded phenotype, yet not necessarily correlated with ICI resistance as demonstrated here, we decided to use spatial transcriptomic datasets to map MBGS (and other molecular subclass signatures) onto tissue sections to observe the immune profile in tumors found to be MBGS-hot. We integrated two previously published HCC spatial transcriptomic datasets which used the 10X Visium platform of 7[31] and 5[32] HCC cases. Following spot integration, normalization, and quality control metrics (see Supplemental Methods), we restricted analysis to 12 (from 11 patients) slides as one slide from Zhang *et al.*[31] did not meet our quality control standards. First, we computed normalized module score expression values for each 10X Visium spot for the Boyault,[21] Chiang,[22] and Hoshida[23] molecular subclassification schemes. Interestingly, across the slides, the Boyault G5/G6 signature highlighted tumor nodules which were also MBGS-hot (Fig. 8a; Fig. S19a). Additionally, nodules which were G1/G2 subclass were exclusive from G3 or G5/G6 or MBGS-hot nodules (Fig. S19a), demonstrating that the Boyault classification is specific to tumor intrinsic signaling. However, the Chiang molecular subclassification demonstrated MBGS-hot tumors overlapped well with tumors which were Chiang_CTNNB1 and Chiang_IFN subclasses (Fig. S20a), with regions in both the tumor nodules and the tissue stroma demonstrating high expression for Chiang_IFN subclass. Hoshida S3 tumors captured nodules which were MBGS-hot, and mutually exclusive to nodules which where Hoshida S1 (Fig. S21a). Moreover, we compared MBGS to previously reported Wnt-CTNNB1 signature[24] and demonstrated that genes

in MBGS had higher overall expression to detect tumor nodules compared with other mutant-Wnt classifiers (Fig. 8b; Fig. S22a). Lastly, we were interested in the immune microenvironment within tumors which were MBGS-hot. Thus, we spatially mapped the expression of Sia *et al.* 'Immune Class' gene signature[33] to the different tissue sections and observed that tumors which were MBGS-hot were immune excluded within the tumor parenchyma, but may exhibit an inflamed stroma in some cases (Fig. 8c; Fig. S23a), which likely contributed to the reported 'Immune-like' subclass[34] in a subset of *CTNNB1*-mutated patients that may show response to ICIs.

Discussion

In the present study, we developed MBGS using multiple mouse models either dependent or non-dependent on β-catenin activation and validated it in several large human HCC integrated genomic-transcriptomic datasets. Aberrant tumor-intrinsic Wnt/β-catenin pathway activation, either through mutations in *CTNNB1, APC,* or *AXIN1*, has been identified in multiple solid tumor types, including HCC, melanoma, colorectal cancer, and endometrial cancer.[35] Activation of this signaling pathway may hold prognostic value in terms of therapy response.[36,37] Most importantly, in the majority of these tumor types, mutated-CTNNB1 has been associated with immune exclusion in the tumor microenvironment,[7,38] which has been categorized as part of the immune excluded subclass in HCC[33,34] and associated with heterogeneous responses to ICIs in both HCC[26,39] and melanoma patients.[40,41] Thus, defining biomarkers of Wnt/β-catenin activity holds diagnostic utility and prognostic implications for eventual treatment selection and stratification as therapies becomes more personalized.

Herein, we developed and characterized two additional SB-HDTVI mouse HCC models to understand tumor biology in representative patient subsets. We have shown here and in previous work that β-M, β-N, β-N-M, and N-M models show greater molecular similarity to respective human HCC subsets with similar perturbations at both the transcriptomic and pathway level.[12,14] Additionally, these models closely mimic the pathophysiology in humans, as demonstrated by the β-N-M model mice requiring euthanasia by about 4–5 weeks and having more Ki67-positive cells compared with the β-M and β-N models; thus mirroring the shorter survival seen in patients with concomitant activation of β-catenin, NRF2, and MET signaling. Notably, we identified an interesting link between β-catenin activation and retinol/retinoate biosynthesis across all models. Retinoic acid is known to modulate expression of NKG2D ligands, which upon binding to NK cells induces cytotoxicity and cytokine secretion.[42,43] In fact, expression of NKG2D ligands (MICA, MICB, ULBP1, and ULBP2) has been reported to be inhibited by β-catenin signaling in HCC.[44]

and scaled gene expression based on z-score is shown. (C) Boxplot of normalized expression values of each individual gene in the 13-gene panel showing enrichment in *CTNNB1*-mutated compared with *CTNNB1*-wild-type and normal tumor liver. Individual values per patient are depicted with bold line in middle representing the median and outside boxes showing inner quartile ranges. One-way ANOVA *p* value for each gene is as follows: *AXIN2* (***p <2.22e-16), *GLUL* (***p <2.22e-16), *LGR5* (***p <2.22e-16), *NKD1* (***p <2.22e-16), *NOTUM* (***p <2.22e-16), *RHBG* (***p <2.22e-16), *SBSPON* (***p <8.24e-6), *SLC1A2* (***p <2.22e-16), *SLC13A3* (***p <2.22e-16), *SP5* (***p <2.22e-16), *TCF7* (***p <2.22e-16), *TEDMM1* (***p <2.22e-16), and *TNFRSF19* (***p <2.22e-16). Levels of significance: *p <0.05, **p <0.001, ***p <0.0001.
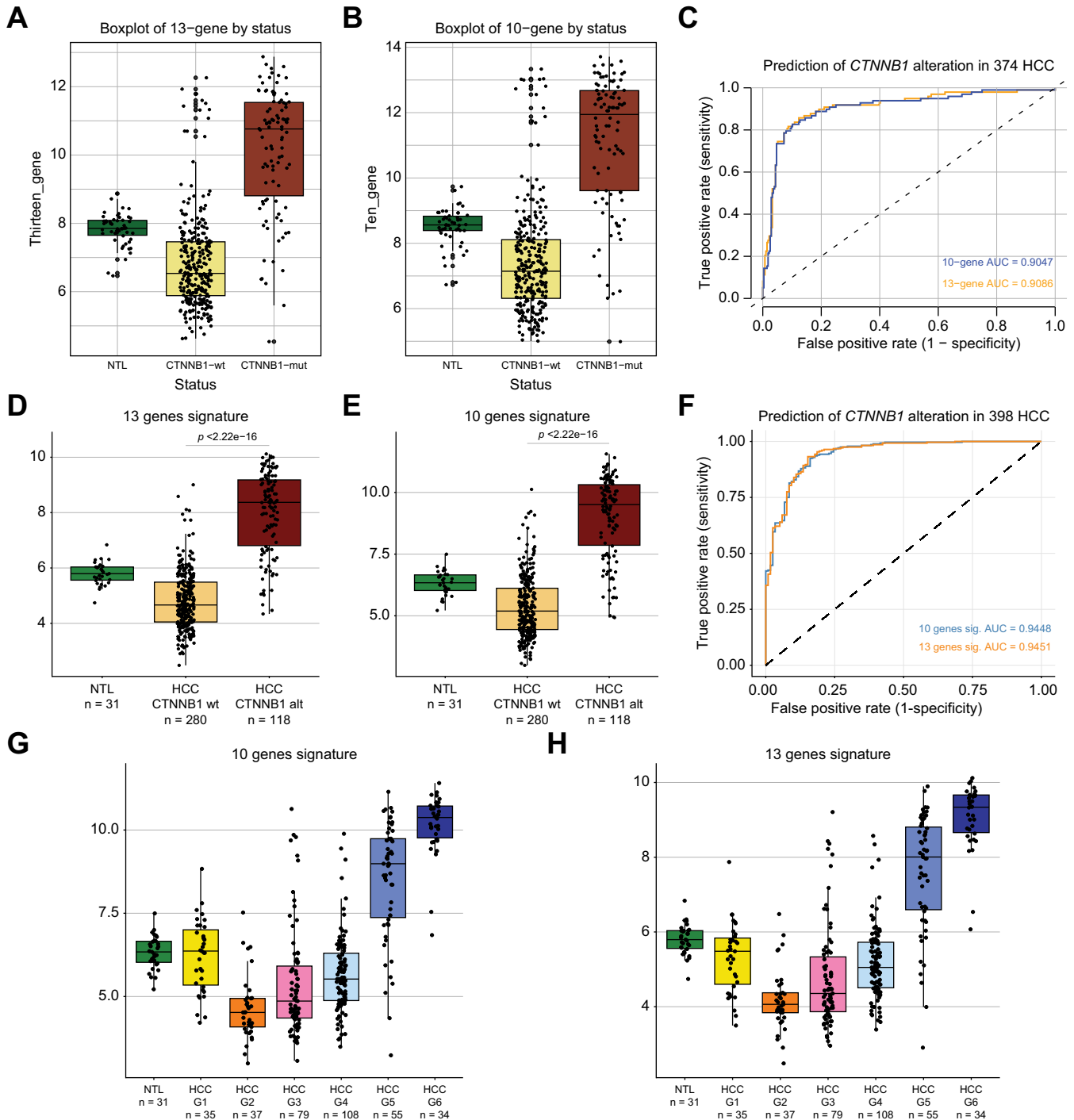
Fig. 6. MBGS classifies *CTNNB1*-mutated HCC with high accuracy. (A) Boxplot of 13-gene mutated-β-catenin gene signature (MBGS) stratified by *CTNNB1*-mutated (n = 98), *CTNNB1*-wild-type (n = 276), and normal tumor liver (n = 50) in The Cancer Genome Atlas-Liver Hepatocellular Carcinoma (TCGA-LIHC). One-way ANOVA *p* value for 13-gene is ***p <2.22e-16. (B) Boxplot of 10-gene MBGS stratified by *CTNNB1*-mutated (n = 98), *CTNNB1*-wild-type (n = 276), and normal tumor liver (n = 50) in TCGA-LIHC. One-way ANOVA *p* value for 10-gene is ***p <2.22e-16. For (A) and (B) Individual values per patient are depicted with bold line in middle representing the median and outside boxes showing inner quartile ranges. (C) AUC/ROC curve showing high sensitivity and specificity to classify *CTNNB1*-mutated cases with 13-gene MBGS of 0.91 and 10-gene MBGS of 0.90 in TCGA-LIHC. (D) Boxplot of 13-gene MBGS stratified by *CTNNB1*-mutated (n = 118), *CTNNB1*-wild-type (n = 280), and normal tumor liver (n = 31) in French cohort. One-way ANOVA *p* value for 13-gene is ***p <2.22e-16. (E) Boxplot of 10-gene MBGS stratified by CTNNB1-mutated (n = 118), CTNNB1-wild-type (n = 280), and normal tumor liver (n = 31) in French cohort. One-way ANOVA *p* value for 13-gene is ***p <2.22e-16. For (E) and (F) Individual values per patient are depicted with bold line in middle representing the median and outside boxes showing inner quartile ranges. (F) AUC/ROC curve showing high sensitivity and specificity to classify CTNNB1-mutated cases with 13-gene MBGS of 0.95 and 10-gene MBGS of 0.94 in French cohort. (G) Stratification of 10-gene MBGS by HCC Hoshida G1-G6 subgroups showing enrichment in G5/G6 groups. (H) Stratification of 13-gene MBGS by HCC Hoshida G1-G6 subgroups showing enrichment in G5/G6 groups. For (G) and (H) Individual values per patient are depicted with the bold line in middle representing the median and outside boxes showing inner quartile ranges; no statistical test was used, but depicted this way for visual representation across the different subclasses. Levels of significance: *p <0.05, **p <0.001, ***p <0.0001.
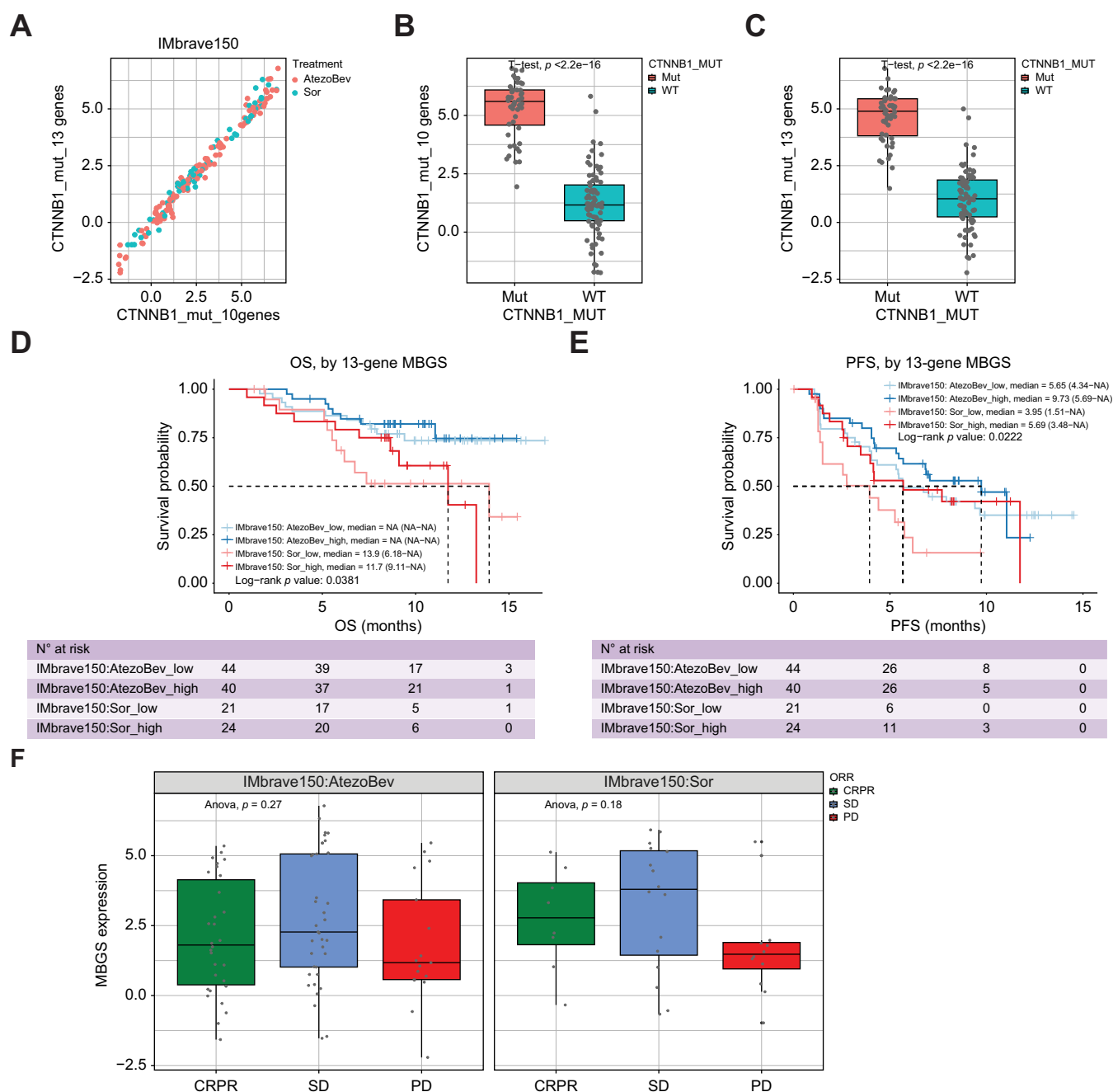
Fig. 7. MBGS predicts relative response to sorafenib in IMbrave150 trial cohort. (A) Correlation based on expression of 10-gene and 13-gene mutated-β-catenin gene signature (MBGS) in IMbrave150 trial cohort. (B) Box plot of expression of 10-gene MBGS in *CTNNB1* wild-type (n = 82) and mutant (n = 48) cases in IMbrave150 cohort. Student's t-test *p* value comparing mutated *vs.* wild-type patients is ****p* <2.22e-16. (C) Box plot of expression of 13-gene MBGS in *CTNNB1* wild-type (n = 82) and mutant (n = 48) cases in the IMbrave150 cohort. Student's t-test *p* value comparing mutated *vs.* wild-type patients is ****p* <2.22e-16. For (B) and (C) Individual values per patient are depicted with bold line in middle representing the median and outside boxes showing inner quartile ranges (D) Kaplan–Meier curve for overall survival demonstrating improved response to sorafenib in MBGS-high patients. Log-rank *p* value is **p* = 0.0381. (E) Kaplan–Meier curve for progression-free survival (PFS) demonstrating improved response to sorafenib in MBGS-high patients. Response to atezolizumab/bevacizumab is comparable between MBGS-high/low patients. Log-rank *p* value is **p* = 0.0222. Log-rank test was used to determine differences in mean survival time. (F) MBGS expression stratified by complete/partial response (CR/PR), stable disease (SD), or progressive disease (PD) defined by mRECIST criteria in each arm. Higher MBGS expression correlated well with sorafenib response. In atezo/bev arm, one-way ANOVA *p* = 0.27. In sorafenib arm, One-way ANOVA *p* = 0.18. For (F), individual values per patient are depicted with bold line in middle representing the median and outside boxes showing inner quartile ranges; no statistical test was used but depicted this way for visual representation across the different subclasses. Levels of significance: **p* <0.05, ***p* <0.001, ****p* <0.0001.

Further, vitamin A, or all-trans retinoic acid (ATRA), used in conjunction with ICI may be effective in tumors with reduced expression of NKG2D ligands,[45] as is the case in β-catenin-mutated HCC.

Another gene identified in MBGS involved in immune exclusion in β-catenin-mutated HCC is tumor necrosis factor receptor superfamily, member 19 (*TNFRSF19*). *TNFRSF19* is part of the TNF-receptor superfamily, a target gene of the Wnt/
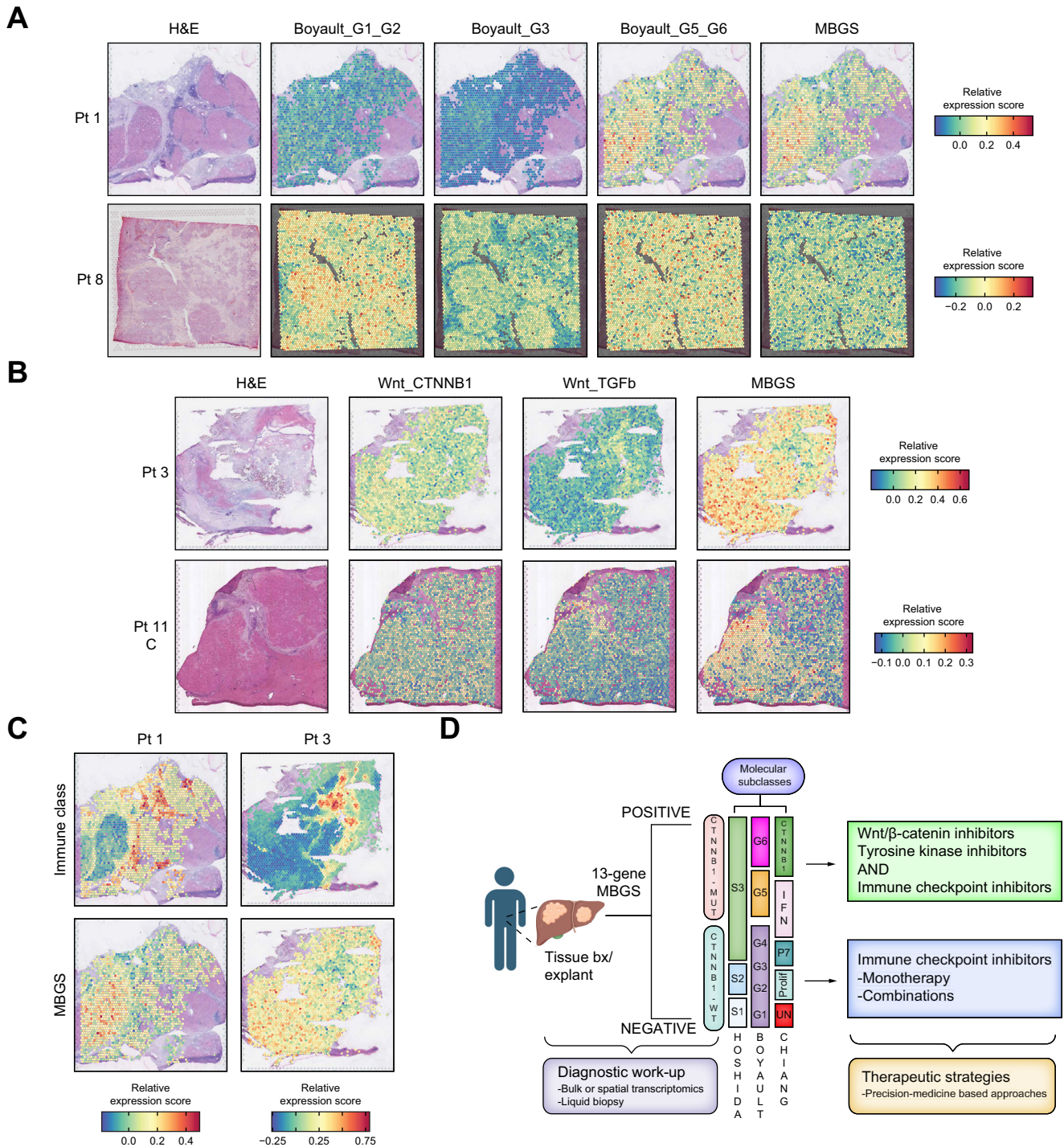
Fig. 8. Spatial mapping of molecular gene signatures reveals MBGS-hot tumors are immune excluded. (A) Representative H&E and spatial gene expression plots of Boyault molecular subclassification and mutated-β-catenin gene signature (MBGS) on same tissue section for a MBGS-hot and MBGS-low tumor. MBGS overlaps with Boyault G5/G6 but is exclusive to Boyault G1/G2 tumors. (B) Representative H&E and spatial gene expression plots of Lachenmayer Wnt signatures and MBGS on same tissue section. Spatial mapping of MBGS highlights tumor nodules more clearly than previously published Wnt-CTNNB1 signatures. (C) Representative H&E and spatial gene expression plots of Sia immune signatures and MBGS on same tissue section. MBGS-hot tumors are immune excluded inside tumor nodules but may have an inflamed stroma. For (A–C), relative expression module scores are depicted with red being higher expression and blue being lower expression. (D) Diagnostic and therapeutic proposed work-up algorithm using MBGS as a companion diagnostic. Patients which are MBGS-high may benefit from anti-β-catenin therapies + ICIs. Figure created using BioRender.com.

β-catenin pathway, and leads to NF-κB activation in Wnt-active cells.[46,47] *TNFRSF19* has been shown to play a role in inhibiting the p38/mitogen-activated protein kinase (MAPK) signaling pathway in the liver.[48] Interestingly, in a recent study, Wong *et al.* demonstrated that NAFLD-associated HCC has an enrichment for *CTNNB1*-mutated HCC with *TNFRSF19* reshaping the immune microenvironment through repression of immunostimulatory cytokines, such as IL6, IL8, CXCL8, CXCL9, and CXCL5.[49] Moreover, response to ICIs could be induced by inhibiting both Wnt signaling (via ICG001) and TNFRSF19 in a mouse model of NAFLD-HCC via orthotopic injection of murine Hepa1-6 cells overexpressing S45P-CTNNB1 on a choline-deficient high fat diet.[49] Whether this signaling axis is sufficient to drive ICI resistance in non-NAFLD *CTNNB1*-mutatd HCC remains to be studied. Future work aimed at testing the direct role of TNFRSF19 in immunocompetent genetic mouse models are needed to further our understanding of this axis as a main driver of immune exclusion in *CTNNB1*-mutated HCC.

It is important to note the discrepancies in association of CTNNB1 mutations with ICI response. Harding *et al.* first reported that patients with HCC having Wnt/β-catenin pathway alterations (with the majority receiving ICI as monotherapy) had worse OS and PFS than those without.[26] A similar observation was made in a study by Ruiz de Galaretta *et al.* through *in vivo* studies and in a small cohort of patients receiving anti-PD-1 therapy.[8] Additionally, Morita *et al.* reported that patients with Wnt activation defined by GS+ IHC had worse OS/PFS on anti-PD-1 therapy.[50] However, work from other groups, albeit in small cohorts as well, have challenged this notion and observed no significant differences in response rates or OS/PFS in patients with or without *CTNNB1* mutations receiving ICI through either profiling pre-treatment biopsy specimens or cell-free DNA.[6,51,52] Re-analysis of the IMbrave150 study results additionally illustrated how patients with and without *CTNNB1* mutations exhibited comparable responses on OS/PFS in the atezo/bev cohort, despite patients with *CTNNB1* mutations having unique responses to sorafenib, which has been illustrated previously.[6,24] *CTNNB1*-mutated patients may be deriving benefit from bevacizumab addition[53] and/or subsets of patients who demonstrate response to ICIs have upregulation of inflammatory gene profiles involved in cytolytic immune activity.[51] This aligns with other studies indicating that patients with *CTNNB1* mutations can be categorized as an 'immune-like' (15% of HCC) or immune excluded (20% of HCC) subclass under the revised immune subclass algorithm, with patients in the 'immune-like' class demonstrating enrichment of antigen type I presentation genes.[34] Through spatial mapping of MBGS and inflamed class gene signatures, this 'immune-like' subclass may in fact be driven by yet unknown microenvironmental features. To reconcile these findings based on previous literature and our findings here, we posit that Wnt/β-catenin signaling may likely be driving immune exclusion within tumors. Yet, unknown mechanisms may influence the development of an inflamed stroma, and inherent tumor-intrinsic ICI resistance mechanisms influenced by oncogenic Wnt signaling may be counterbalanced by tumors harboring engaged interferon signaling or antigen presentation machinery. Thus, further clinical studies in larger cohorts and mechanistic studies are needed to dissect the exact tumor intrinsic and extrinsic features driving different immune phenotypes in *CTNNB1*-mutated HCC leading to the observed heterogenous ICI responses.

Unsurprisingly, another common pathway identified in our gene signature was Glutamine biosynthesis. We have previously shown addiction to mutated-β-catenin-GLUL-glutamine-mTORC1 axis in multiple preclinical models of β-catenin-mutated HCC.[13,14] Indeed, these models are sensitive to mTOR inhibitors, such as everolimus or rapamycin.[13,14] The Everolimus for Liver Cancer Evaluation (EVOLVE-1) trial, which tested everolimus to placebo in patients with HCC in second-line setting, failed to demonstrate any significant survival difference. However, treatment was not restricted to mTOR-addicted tumors as this may have led to more favorable outcomes through screening for patients with either tissue or liquid biopsy-proven β-catenin mutated HCC or tumors with loss of tuberous sclerosis complex 2 (TSC2), which both lead to increased mTOR signaling.[54,55] Thus, subsets of patients with mTOR-addicted tumors may benefit from mTOR inhibitors in neoadjuvant or adjuvant settings. With NIH Cancer Therapy Evaluation Program (CTEP) designation of a novel mTORC1/2 inhibitor, sapanisertib (MLN0128/TAK228), this drug may prove to be efficacious in treating mTOR-addicted HCC tumors given its broad mechanism of action, as has been shown in other solid tumors, including renal, endometrial, and bladder cancer.[56–58] In mouse models of liver cancer, sapanisertib has shown efficacy in HCC with β-catenin activity.[59–61] In fact, in a HCC preclinical model of β-M, combination of sapanisertib with MET inhibitor (cabozantinib) led to tumor regression over three treatment weeks.[59] Thus, future studies testing sapanisertib as monotherapy or in combination with other targeted therapies may provide preclinical rationale for a rational clinical trial testing sapanisertib in patients with HCC with biopsy-proven β-catenin-mutated HCC, such as using MBGS as a companion diagnostic.

Moreover, these SB-HDTVI HCC models are useful systems to identify unique biomarkers. Given the 'inside-out' approach of these models, through dual oncogene induction, and use of immunocompetent mice, these tumor mouse models are useful to test targeted therapies and systemic agents, including sorafenib, mTOR inhibitors, and ICIs, and monitor their biological responses.[8,13,14,62] In fact, we and others have previously shown mechanisms of response to various c-MET inhibitors in the β-M model,[59,63,64] along with studying mechanisms following directed β-catenin inhibition via siRNA therapeutics in multiple β-catenin-driven models, including the mutant-β-catenin/KRAS model.[11,65] As liver tumor biopsies (both tissue and/or liquid) are increasingly becoming more common for identifying oncologic actionable targets for patients,[15] along with the increasing number of molecular pathology laboratories expanding their capacity to perform whole transcriptome testing on patient tissues, developing biomarkers of response becomes ever more crucial in patient molecular stratification for optimal selection of first-line ICI-based treatment regimens. However, there is currently no clinically approved biomarker to guide precision medicine. Immunohistochemical staining for programmed death-ligand 1 protein expression in HCC has not translated well for predicting ICI response compared with its use in other tumor types.[66] RNA based assays, including transcriptomic profiling, have already yielded promising results

to predict response,[51] including our study here. Thus, gene signatures may prove crucial to aid in patient molecular stratification in both the neoadjuvant and adjuvant settings post-resection or transplantation.[67,68]

Several limitations of MBGS and this study need to be addressed. First, we did not assess MBGS value as a liquid biopsy based biomarker as these are becoming increasingly clinically relevant for HCC.[15] It would be interesting to test whether cell-free RNAs of MBGS genes are present in serum/plasma of *CTNNB1*-mutated patients at higher abundance compared with *CTNNB1* WT patients. Additionally, NOTUM and TNFRSF19 are both secreted proteins with ELISA assays available; thus, it would be worthwhile to assess their presence in serum/plasma of patients with HCC. Second, we did not have matched whole-exome sequencing data available for the patients included in the spatial transcriptomic analysis. Therefore, we could not confirm that MBGS captured CTNNB1-mutated patients here, but rather used this analysis to ascertain the tumor intrinsic and extrinsic components of the various molecular subclass gene signatures. Lastly, we did not prospectively validate MBGS in a separate cohort and compare to GS immunohistochemistry, which is the gold standard for

diagnosing *CTNNB1*-mutated cases. This would be needed prior to advancing MBGS as a companion diagnostic in the clinic.

In summary, the MBGS panel could assist in diagnosing an important HCC molecular subset, which demonstrates heterogenous responses to first-line ICI combinations. Ultimately, it would aid in patient selection for precision therapy using whole or spatial transcriptomics and data from additional innovative technological platforms as molecular testing becomes more desirable and routine in HCC. Specifically, the application of MBGS would be most desirable where transcriptomic platforms are utilizing fewer genes in their panels (e.g., NanoString, Molecular Cartography[TM]). Furthermore, as digital pathology and artificial intelligence-based machine learning becomes integrated into molecular diagnostics laboratories, there will be opportunities for MBGS-like panels to be instructive. Therapies employing TKIs, mTOR inhibitors, and anti-β-catenin therapies alone or in combination with ICIs have already shown to benefit CTNNB1-mutated HCC in preclinical models and are awaiting clinical validation (Fig. 8d).[69,70] Having tools such as MBGS to serve as a companion diagnostic will expedite precision trials and successful translation into clinical medicine.

Affiliations

[1]*Department of Pharmacology and Chemical Biology, University of Pittsburgh School of Medicine, Pittsburgh, PA, USA;* [2]*Pittsburgh Liver Research Center, University of Pittsburgh and University of Pittsburgh Medical Center, Pittsburgh, PA, USA;* [3]*Medical Scientist Training Program, University of Pittsburgh, Pittsburgh, PA, USA;* [4]*Centre de Recherche des Cordeliers, Université Paris Cité, Sorbonne Université, Inserm, Paris, France;* [5]*Institut du Cancer Paris CARPEM, AP-HP, Department of Oncology, Hopital Européen Georges Pompidou, Paris, France;* [6]*Translational Medicine, Genentech Inc., San Francisco, CA, USA;* [7]*Department of Pathology, University of Pittsburgh Medical Center, Pittsburgh, PA, USA;* [8]*Division of Gastroenterology, Hepatology and Nutrition, Department of Medicine, University of Pittsburgh School of Medicine, Pittsburgh, PA, USA*

Abbreviations

CR/PR, complete/partial response; DEG, differentially expressed gene, DGE, Differential gene expression; FC, Fold Change; FDR, false discovery rate; GOF, gain-of-function; GS, glutamine synthetase; HCC, hepatocellular carcinoma; ICI, immune checkpoint inhibitor; IHC, immunohistochemistry; LIHC, liver hepatocellular carcinoma; LOF, loss of function; MBGS, mutated-β-catenin gene signature; NRF2, Nuclear-factor-like 2; OS, overall survival; PD, progressive disease; PFS, progression-free survival; SB-HDTVI, sleeping beauty transposon/transposase and hydrodynamic tail vein injection; SD, stable disease.

Conflicts of interest

SPM has received research grants from Alnylam Pharmaceuticals and Fog Pharmaceuticals and is a consultant for and on Advisory Boards for Surrozen, AntlerA, Alnylam, Mermaid Bio, Vicero Inc, and UbiquiTx. However, there is no pertinent conflicts of interest related to the current manuscript. YW, XG and SL are employed by Genentech Inc., San Francisco, CA. No other authors have any relevant conflicts of interests to declare regarding the current study.

Please refer to the accompanying ICMJE disclosure forms for further details.

Authors' contributions

Conceived the study, funded the study, helped performed analysis and interpretation, edits and finalizing manuscript: SPM. Conceived the study, performed and executed the study, performed analysis and statistics and wrote the first draft of the manuscript: BML. Helped perform analysis on partial patient datasets, generate figures, statistical analysis on partial patient data and helped write part of the study: LP, TZH. Helped perform analysis on patient datasets, generate figures and help perform statistical analysis on partial patient data: XG, SL. Helped perform computational analysis and helped with statistical analysis as well as helped write part of the study: SL, TMY. Helped perform part of the study and help with analysis on part of the study: ERD. Helped with generation of animal models, helped execute technical aspects of the study and performed partial analysis of the study: JT. Helped with technical aspects on part of the study and help with analysis: YL,SS, MP, AB, CC. Helped with troubleshooting, writing and interpretation of clinical data and intellectual insight into clinical aspects of the

study: ADS, YW. Helped with troubleshooting, writing and interpretation of patient data and analysis and intellectual insight into clinical aspects of the study: JZR.

Data availability statement

Transcriptomic data for the HCC animal models has been made available through gene expression omnibus under accession number: GSE261316. All other human datasets have been made available previously and accession numbers are in the Methods.

Declaration of Generative AI and AI-assisted technologies in the writing process

During the preparation of this work the authors used ChatGPT-3.5 in order to assist with debugging of some R packages that had lack of in-depth user documentation in their vignettes. After using this tool/service, the authors reviewed and edited the content as needed and take full responsibility for the content of the publication.

Supplementary data

Supplementary data to this article can be found online at https://doi.org/10.1016/j.jhepr.2024.101186.

References

Author names in bold designate shared co-first authorship

[1] Sung H, Ferlay J, Siegel RL, et al. Global cancer statistics 2020: GLOBOCAN estimates of incidence and mortality worldwide for 36 cancers in 185 countries. CA Cancer J Clin 2021;71:209–249.

[2] Toh MR, Wong EY, Wong SH, et al. Global epidemiology and genetics of hepatocellular carcinoma. Gastroenterology 2023;164:766–782.

[3] Llovet JM, Zucman-Rossi J, Pikarsky E, et al. Hepatocellular carcinoma. Nat Rev Dis Primers 2016;2:16018.

[4] Cheng AL, Qin S, Ikeda M, et al. Updated efficacy and safety data from IMbrave150: atezolizumab plus bevacizumab vs. sorafenib for unresectable hepatocellular carcinoma. J Hepatol 2022;76:862–873.

[5] **Abou-Alfa GK**, **Lau G**, **Kudo M**, et al. Tremelimumab plus durvalumab in unresectable hepatocellular carcinoma. NEJM Evid 2022;1:EVIDoa2100070.

[6] Zhu AX, Abbas AR, de Galarreta MR, et al. Molecular correlates of clinical response and resistance to atezolizumab in combination with bevacizumab in advanced hepatocellular carcinoma. Nat Med 2022;28:1599–1611.

[7] Luke JJ, Bao R, Sweis RF, et al. WNT/beta-catenin pathway activation correlates with immune exclusion across human cancers. Clin Cancer Res 2019;25:3074–3083.

[8] Ruiz de Galarreta M, Bresnahan E, Molina-Sánchez P, et al. Beta-catenin activation promotes immune escape and resistance to anti-PD-1 therapy in hepatocellular carcinoma. Cancer Discov 2019;9:1124–1141.

[9] **Schulze K**, **Imbeaud S**, **Letouzé E**, et al. Exome sequencing of hepatocellular carcinomas identifies new mutational signatures and potential therapeutic targets. Nat Genet 2015;47:505–511.

[10] Cancer Genome Atlas Research Network. Comprehensive and integrative genomic characterization of hepatocellular carcinoma. Cell 2017;15(169):1327–1341. e23.

[11] Tao J, Zhang R, Singh S, et al. Targeting beta-catenin in hepatocellular cancers induced by coexpression of mutant beta-catenin and K-Ras in mice. Hepatology 2017;65:1581–1599.

[12] Tao J, Xu E, Zhao Y, et al. Modeling a human hepatocellular carcinoma subset in mice through coexpression of met and point-mutant beta-catenin. Hepatology 2016;64:1587–1605.

[13] **Adebayo Michael AO**, **Ko S**, Tao J, et al. Inhibiting glutamine-dependent mTORC1 activation ameliorates liver cancers driven by beta-catenin mutations. Cell Metab 2019;29:1135–1150. e6.

[14] Tao J, Krutsenko Y, Moghe A, et al. Nuclear factor erythroid 2-related factor 2 and beta-catenin coactivation in hepatocellular cancer: biological and therapeutic implications. Hepatology 2021;74:741–759.

[15] **Lehrich BM**, **Zhang J**, Monga SP, et al. Battle of the Biopsies: role of tissue and liquid biopsy in hepatocellular carcinoma. J Hepatol 2024;80:515–530.

[16] **Goldstein LD**, **Lee J**, Gnad F, et al. Recurrent loss of NFE2L2 Exon 2 is a mechanism for Nrf2 pathway activation in human cancers. Cell Rep 2016;16:2605–2617.

[17] Kaposi-Novak P, Lee JS, Gòmez-Quiroz L, et al. Met-regulated expression signature defines a subset of human hepatocellular carcinomas with poor prognosis and aggressive phenotype. J Clin Invest 2006;116:1582–1595.

[18] **Subramanian A**, **Tamayo P**, Mootha VK, et al. Gene set enrichment analysis: a knowledge-based approach for interpreting genome-wide expression profiles. Proc Natl Acad Sci U S A 2005;102:15545–15550.

[19] **Rebouissou S**, **Franconi A**, Calderaro J, et al. Genotype-phenotype correlation of CTNNB1 mutations reveals different ß-catenin activity associated with liver tumour progression. Hepatology 2016;64:2047–2061.

[20] Tobin RP, Cogswell DT, Cates VM, et al. Targeting MDSC differentiation using ATRA: a Phase I/II clinical trial combining pembrolizumab and all-trans retinoic acid for metastatic melanoma. Clin Cancer Res 2023;29:1209–1219.

[21] **Boyault S**, **Rickman DS**, **de Reyniès A**, et al. Transcriptome classification of HCC is related to gene alterations and to new therapeutic targets. Hepatology 2007;45:42–52.

[22] Chiang DY, Villanueva A, Hoshida Y, et al. Focal gains of VEGFA and molecular classification of hepatocellular carcinoma. Cancer Res 2008;68:6779–6788.

[23] Hoshida Y, Nijman SM, Kobayashi M, et al. Integrative transcriptome analysis reveals common molecular subclasses of human hepatocellular carcinoma. Cancer Res 2009;69:7385–7392.

[24] **Lachenmayer A**, **Alsinet C**, Savic R, et al. Wnt-pathway activation in two molecular classes of hepatocellular carcinoma and experimental modulation by sorafenib. Clin Cancer Res 2012;18:4997–5007.

[25] Nault JC, Martin Y, Caruso S, et al. Clinical impact of genomic diversity from early to advanced hepatocellular carcinoma. Hepatology 2020;71:164–182.

[26] **Harding JJ**, **Nandakumar S**, Armenia J, et al. Prospective genotyping of hepatocellular carcinoma: clinical implications of next-generation sequencing for matching patients to targeted and immune therapies. Clin Cancer Res 2019;25:2116–2126.

[27] Li B, Li Y, Zhou H, et al. Multiomics identifies metabolic subtypes based on fatty acid degradation allocating personalized treatment in hepatocellular carcinoma. Hepatology 2024;79:289–306.

[28] Ayers M, Lunceford J, Nebozhyn M, et al. IFN-gamma-related mRNA profile predicts clinical response to PD-1 blockade. J Clin Invest 2017;127:2930–2940.

[29] **Jiang P**, **Gu S**, **Pan D**, et al. Signatures of T cell dysfunction and exclusion predict cancer immunotherapy response. Nat Med 2018;24:1550–1558.

[30] **Cabrita R**, **Lauss M**, Sanna A, et al. Tertiary lymphoid structures improve immunotherapy and survival in melanoma. Nature 2020;577(7791):561–565.

[31] Zhang S, Yuan L, Danilova L, et al. Spatial transcriptomics analysis of neoadjuvant cabozantinib and nivolumab in advanced hepatocellular carcinoma identifies independent mechanisms of resistance and recurrence. Genome Med 2023;15:72.

[32] **Wu R**, **Guo W**, **Qiu X**, et al. Comprehensive analysis of spatial architecture in primary liver cancer. Sci Adv 2021;7:eabg3750.

[33] Sia D, Jiao Y, Martinez-Quetglas I, et al. Identification of an immune-specific class of hepatocellular carcinoma, based on molecular features. Gastroenterology 2017;153:812–826.

[34] **Montironi C**, **Castet F**, **Haber PK**, et al. Inflamed and non-inflamed classes of HCC: a revised immunogenomic classification. Gut 2023;72:129–140.

[35] Kim S, Jeong S. Mutation hotspots in the beta-catenin gene: lessons from the human cancer genome databases. Mol Cell 2019;42:8–16.

[36] Wang J, Zhu G. A precise prognostic signature in CTNNB1-mutant hepatocellular carcinoma: prognosis prediction and precision treatment exploration. Heliyon 2023;9:e22382.

[37] **Hollis RL**, **Thomson JP**, **Stanley B**, et al. Molecular stratification of endometrioid ovarian carcinoma predicts clinical outcome. Nat Commun 2020;11:4995.

[38] Fujita M, Yamaguchi R, Hasegawa T, et al. Classification of primary liver cancer with immunosuppression mechanisms and correlation with genomic alterations. EBiomedicine 2020;53:102659.

[39] **Chen L**, **Zhou Q**, Liu J, Zhang W. CTNNB1 Alternation is a potential biomarker for immunotherapy prognosis in patients with hepatocellular carcinoma. Front Immunol 2021;12:759565.

[40] Spranger S, Bao R, Gajewski TF. Melanoma-intrinsic beta-catenin signalling prevents anti-tumour immunity. Nature 2015;523(7559):231–235.

[41] Nsengimana J, Laye J, Filia A, et al. Beta-catenin-mediated immune evasion pathway frequently operates in primary cutaneous melanomas. J Clin Invest 2018;128:2048–2063.

[42] Cerwenka A, Bakker AB, McClanahan T, et al. Retinoic acid early inducible genes define a ligand family for the activating NKG2D receptor in mice. Immunity 2000;12:721–727.

[43] Poggi A, Catellani S, Garuti A, et al. Effective in vivo induction of NKG2D ligands in acute myeloid leukaemias by all-trans-retinoic acid or sodium valproate. Leukemia 2009;23:641–648.

[44] Cadoux M, Caruso S, Pham S, et al. Expression of NKG2D ligands is downregulated by beta-catenin signalling and associates with HCC aggressiveness. J Hepatol 2021;74:1386–1397.

[45] Rao A, Zhang X, Kim J, et al. TMIC-13. Efficacy of retinoic acid in reversing immune evasion in IDH mutant gliomas. Neuro-Oncology 2018;20(Suppl 6).vi258-vi258.

[46] Qiu W, Hu Y, Andersen TE, et al. Tumour necrosis factor receptor superfamily member 19 (TNFRSF19) regulates differentiation fate of human mesenchymal (stromal) stem cells through canonical Wnt signaling and C/EBP. J Biol Chem 2010;285:14438–14449.

[47] Schön S, Flierman I, Ofner A, et al. β-catenin regulates NF-κB activity via TNFRSF19 in colorectal cancer cells. Int J Cancer 2014;135:1800–1811.

[48] Zhang Y, Zhang X, Chen R, et al. Hepatic stellate cell-derived exosome miR-122-5p targets TNFRSF19 to inhibit EMT and fibrosis in intrahepatic biliary epithelial cells via the p38 MAPK pathway. https://doi.org/10.21203/rs.3.rs-2997966/v1.

[49] **Wong AM**, **Ding X**, Wong AM, et al. Unique molecular characteristics of NAFLD-associated liver cancer accentuate beta-catenin/TNFRSF19-mediated immune evasion. J Hepatol 2022;77:410–423.

[50] Morita M, Nishida N, Sakai K, et al. Immunological microenvironment predicts the survival of the patients with hepatocellular carcinoma treated with anti-PD-1 antibody. Liver Cancer 2021;10:380–393.

[51] Haber PK, Castet F, Torres-Martin M, et al. Molecular markers of response to anti-PD1 therapy in advanced hepatocellular carcinoma. Gastroenterology 2023;164:72–88. e18.

[52] von Felden J, Craig AJ, Garcia-Lezana T, et al. Mutations in circulating tumour DNA predict primary resistance to systemic therapies in advanced hepatocellular carcinoma. Oncogene 2021;40:140–151.

[53] Ogawa K, Kanzaki H, Chiba T, et al. Effect of atezolizumab plus bevacizumab in patients with hepatocellular carcinoma harbouring CTNNB1 mutation in early clinical experience. J Cancer 2022;13:2656–2661.

[54] Zhu AX, Kudo M, Assenat E, et al. Effect of everolimus on survival in advanced hepatocellular carcinoma after failure of sorafenib: the EVOLVE-1 randomized clinical trial. JAMA 2014;312:57–67.

[55] Huynh H, Hao HX, Chan SL, et al. Loss of tuberous sclerosis Complex 2 (TSC2) is frequent in hepatocellular carcinoma and predicts response to mTORC1 inhibitor everolimus. Mol Cancer Ther 2015;14:1224–1235.

[56] Voss MH, Gordon MS, Mita M, et al. Phase 1 study of mTORC1/2 inhibitor sapanisertib (TAK-228) in advanced solid tumours, with an expansion phase in renal, endometrial or bladder cancer. Br J Cancer 2020;123:1590–1598.

[57] Subbiah V, Coleman N, Piha-Paul SA, et al. Phase I study of mTORC1/2 inhibitor sapanisertib (CB-228/TAK-228) in combination with metformin in patients with mTOR/AKT/PI3K pathway alterations and advanced solid malignancies. Cancer Res Commun 2024;4:378–387. PMID 38126764.

[58] Han SN, Oza A, Colombo N, et al. A randomized phase 2 study of sapanisertib in combination with paclitaxel *vs.* paclitaxel alone in women with advanced, recurrent, or persistent endometrial cancer. Gynecol Oncol 2023;178:110–118.

[59] Shang R, Song X, Wang P, et al. Cabozantinib-based combination therapy for the treatment of hepatocellular carcinoma. Gut 2021;70:1746–1757.

[60] Zhang S, Song X, Cao D, et al. Pan-mTOR inhibitor MLN0128 is effective against intrahepatic cholangiocarcinoma in mice. J Hepatol 2017;67:1194–1203.

[61] Song X, Liu X, Wang H, et al. Combined CDK4/6 and Pan-mTOR inhibition is synergistic against intrahepatic cholangiocarcinoma. Clin Cancer Res 2019;25:403–413.

[62] Liu X, Hu J, Song X, et al. Combined treatment with MEK and mTOR inhibitors is effective in in vitro and in vivo models of hepatocellular carcinoma. Cancers (Basel) 2019;11(7).

[63] Zhan N, Michael AA, Wu K, et al. The effect of selective c-MET inhibitor on hepatocellular carcinoma in the MET-active, beta-catenin-mutated mouse model. Gene Expr 2018;18:135–147.

[64] Wang H, Zhou Y, Xu H, et al. Therapeutic efficacy of FASN inhibition in preclinical models of HCC. Hepatology 2022;76:951–966.

[65] Ganesh S, Koser ML, Cyr WA, et al. Direct pharmacological inhibition of beta-catenin by RNA interference in tumours of diverse origin. Mol Cancer Ther 2016;15:2143–2154.

[66] Pinato DJ, Mauri FA, Spina P, et al. Clinical implications of heterogeneity in PD-L1 immunohistochemical detection in hepatocellular carcinoma: the Blueprint-HCC study. Br J Cancer 2019;120:1033–1036.

[67] Llovet JM, Castet F, Heikenwalder M, et al. Immunotherapies for hepatocellular carcinoma. Nat Rev Clin Oncol 2022;19:151–172.

[68] Llovet JM, Pinyol R, Yarchoan M, et al. Adjuvant and neoadjuvant immunotherapies in hepatocellular carcinoma. Nat Rev Clin Oncol 2024;21:294–311.

[69] Rialdi A, Duffy M, Scopton AP, et al. WNTinib is a multi-kinase inhibitor with specificity against beta-catenin mutant hepatocellular carcinoma. Nat Cancer 2023;4:1157–1175.

[70] Saito Y, Yin D, Kubota N, et al. A therapeutically targetable TAZ-TEAD2 pathway drives the growth of hepatocellular carcinoma via ANLN and KIF23. Gastroenterology 2023;164:1279–1292.